ELSEVIER

International Journal of Minerals, Metallurgy and Materials
Volume 16, Number 2, April 2009, Page 208

Materials

Characterization of Fe_3Si-based coatings on low silicon steel by pulsed Nd:YAG laser cladding

Dan-yang Dong[1,2], *Chang-sheng Liu*[1], *Sui-yuan Chen*[1], *and Bin Zhang*[1]

1) Key Laboratory for Anisotropy and Texture of Materials of the Ministry of Education of China, Northeastern University, Shenyang 110004, China
2) School of Science College, Northeastern University, Shenyang 110004, China
(Received 2008-04-26)

Abstract: The Fe_3Si based coating was produced on the Fe-1Si steel surface by a pulsed Nd:YAG (yttrium aluminum garnet) laser. Its phase constitution and microstructure were characterized by using X-ray diffraction (XRD), optical microscope (OM), and field emission scanning electron microscope (FESEM) with associated energy dispersive spectroscopy (EDS) and transmission electron microscopy (TEM). The hyperfine structure of the coating was studied by Mössbauer spectra (MS) and the magnetic property was also measured at room temperature by a vibrating sample magnetometer (VSM). The obtained coating is pore and crack-free with dense microstructure and high Si content. The metallurgical bonding between the coating and the substrate was realized. The microstructure of the coating is typical fine dendrites. The major phase was confirmed by XRD and TEM to be the ordering $D0_3$ structured Fe_3Si phase. In addition, there were smaller amounts of the Fe_5Si_3 phase and the γ-Fe phase in the coating. Compared with the substrate, the laser cladding coating has a lower saturation magnetization and a higher coercive force. The poor magnetic property might be because of rapid solidification microstructure and phase constitution in the coating.

Key words: silicon steel; laser cladding; hyperfine structure; magnetic property

[*This study was financially supported by the National Natural Science Foundation of China (No.50474084).*]

1. Introduction

It is well known that increasing the Si content improves the soft magnetic properties of silicon steel. However, increasing the Si content makes the steel brittle [1-2]. Laser cladding is a process, in which an alloy powder of a desired composition is melted with minimum mixing to the substrate under laser irradiation and then rapidly solidifies to form a dense coating with refined microstructure and metallurgical bonding to the substrate. A relatively high rate of processing, ease of automation, possible operation under atmospheric pressure, and the localized nature of laser treatment are additional advantages [3].

Previous studies by the present authors have proved that obtaining the high Si content or high Si gradient silicon steel by Nd:YAG (yttrium aluminum garnet) laser cladding on the low silicon steel surface followed by diffusion annealing is feasible [4-5]. In the present work, a higher Si content coating, which was mainly composed of Fe_3Si, was produced under the optimized parameters by the pulsed Nd:YAG laser cladding process. The emphasis of this work was put on the characterization of phase constitution, microstructure, and the hyperfine structure of this kind of Fe_3Si-based coating, which was expected to give more Si atoms to the Fe-1Si substrate during the subsequent diffusion annealing to produce the silicon steel with high Si content. The magnetic property of the obtained cladding coating was also measured at room temperature (RT).

2. Experimental

Fig. 1 shows the schematic diagram of the cladding process performed in this study. The hot-rolled non-oriented silicon steel with the chemical composition (wt%) of 1 Si, 0.20 Mn, 0.28 Al, 0.005 C, and balance Fe was used as a substrate material for the laser cladding process. The specimens were 50 mm×15 mm×2.65 mm in dimension and the surface of the

Corresponding author: Dan-yang Dong, **E-mail:** danyangdong@gmail.com
Also available online at www.sciencedirect.com

specimens was sand-blasted in order to roughen the surface to enhance powder adhesion prior to laser cladding. The powders used for laser cladding were Fe (particle size: 75 μm) and Si (particle size: 75 μm). These powders were mixed as a pre-placed powder bed on the substrate according to the mass fraction ratios of Fe:Si=2:3. The thickness of the powder bed was fixed to 0.5 mm.

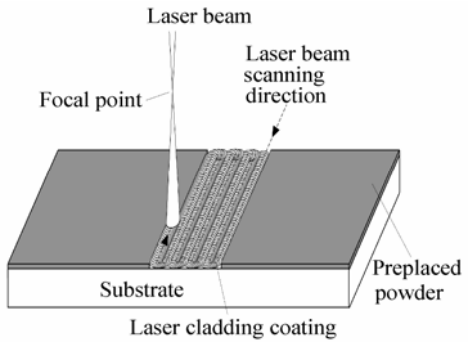

Fig. 1. Schematic diagram of the multi-track laser cladding process.

The pulsed Nd:YAG laser beam (JHM-1GY-400 type) with the focus length of 100 mm and the wavelength of 1.064 μm was irradiated on the specimen surface in the multi-track mode. The substrate was moved by an auto-controlled table under the stationary laser beam. The excellent cladding coating obtained should be free from pore, crack, and have a relatively smooth surface. The laser cladding conditions were determined after preliminary experiments and the optimized parameters are listed in Table 1.

Table 1. Optimized laser cladding parameters in the present study

Laser power / J	24.8
Pulse frequency / Hz	15
Pulse width / ms	3.0
Laser scanning rate / ($mm \cdot s^{-1}$)	2.5
Spot diameter / mm	1.44
Focus length / mm	100
Defocus / mm	18
Thickness of preplaced coating / mm	0.5
Spot overlapping ratio / %	50

After laser cladding, the phase identifications were conducted along the depth of the cladding coating by X-ray diffractometer (XRD, X'Pert Pro MPD-PW3040/60 type) in 2θ mode with Cu K_α radiation at 40 kV and 40 mA. The microstructures were characterized by optical microscope (OM, Olympus-GX71 type), field emission scanning electron microscope (FESEM, Supra 35 type) with back scattered electron (BSE) imaging, equipped with an Oxford energy dispersive spectroscopy (EDS) and transmission electron microscopy (TEM, Tecnai G^2 20 type), with the acceleration voltage of 200 kV. The specimens for TEM analysis were cut along the direction perpendicular to the cross section of the multi-track laser cladding coating, and the TEM thin foils were prepared by standard twin-jet electro-polishing using a 6vol% perchloric acid and 94vol% methanol electrolyte at 248 K. The Mössbauer spectra (MS) of the Fe-1Si substrate and laser cladding coating were recorded in transmission geometry at RT using a spectrometer (FH-1918 type) with constant acceleration, and the source of γ-emission was ^{57}Co in Pd. The calibration was performed with an α-Fe foil. The spectra were fitted and decomposed into subspectra by the Msu8 program. The cladding coating was cut along the interface between the coating and the substrate, and the measurement of magnetic property was performed on a Lake Shore 7407 vibrating sample magnetometer (VSM) with the magnetic field applied vertical to the coating.

3. Results and discussion

3.1. Phase constitution of the laser cladding coating

The cladding coating prepared under the optimized parameters shown in Table 1 shows good surface quality, which is free from macrocracks and macropores.

Fig. 2 presents the X-ray diffraction spectra along the depth of the laser cladding coating. The diffraction peaks of Fe_3Si were present on the cladding surface and in the middle part of the cladding coating. XRD spectra reveal the existence of $D0_3$ structured Fe_3Si phase with the characteristic peak of (200) [6-7]. In addition, it is found from Fig. 2 that there are also a small amount of Fe_5Si_3 and γ-Fe in the cladding coating. Consequently, it might be concluded that the coating is mainly composed of Fe_3Si phase.

3.2. Microstructure of the laser cladding coating

Fig. 3 shows the cross-sectional OM micrographs of the cladding coating. Fig. 4 is the SEM BSE micrograph of the laser cladding coating and the EDS analysis of the Fe and Si content in dendritic and interdendritic zones, and in the interface zone, respectively.

Typically, there exist three characteristic zones along the depth of the coating including the CZ, IZ, and HAZ as shown in Fig. 3. The dendrites near the interface between the cladding coating and the substrate show vertical alignment, which indicates that a vertical temperature gradient as heat is conducted away from the melt pool towards the substrate. And

there are the disoriented and finer dendrites near the top surface. The interface zone between the cladding coating and the substrate is a bright strip observed under optical microscopy (Fig. 3(c)). The bright strip is a planar front solidified layer, which is epitaxially grown from the substrate. The EDS analysis of the interface zone (Fig. 4(d)) shows the Si content of the interface zone is 10.67wt%, and the phase of the interface zone identified by XRD spectra is α-Fe(Si) solution as shown in Fig. 2(c). Based on the results above, the formation of the excellent metallurgical bonding between the cladding coating and the substrate can be confirmed. The HAZ is characterized by a fine martensite. More details of solidified microstructure evolution had been presented in our previous work [4-5].

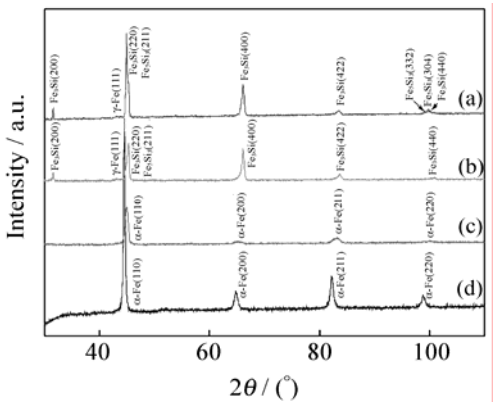

Fig. 2. XRD spectra of the cladding coating surface (a), middle part of the cladding coating (b), interface between the coating and the substrate (c), and the Fe-1Si substrate (d).

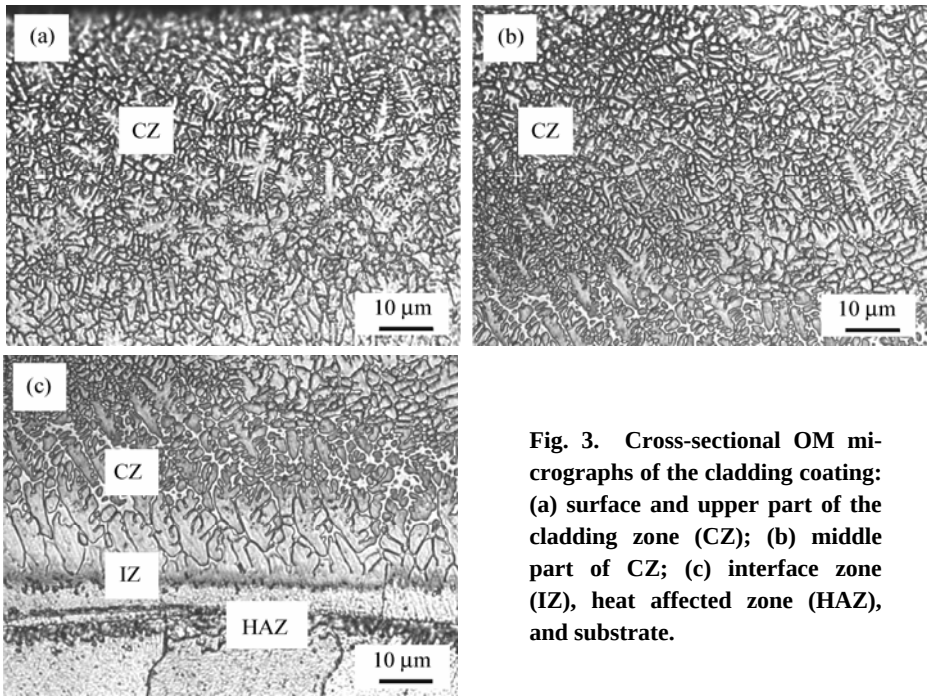

Fig. 3. Cross-sectional OM micrographs of the cladding coating: (a) surface and upper part of the cladding zone (CZ); (b) middle part of CZ; (c) interface zone (IZ), heat affected zone (HAZ), and substrate.

Figs. 3 and 4 reveal that the solidification microstructure of the laser cladding coating presented the dendritic and interdendritic growth morphologies. The Fe and Si contents of dendrite and interdendrite were performed by the EDS spot scanning analysis, as shown in Figs. 4(b) and 4(c). The results show that the Si contents of dendrite and interdendrite reach as high as 15.20wt% and 13.86wt%, respectively. The mass fractions of dendrites and interdendrites suggest that the coating is mainly composed of the Fe_3Si phase, in agreement with the phase diagram of Fe-Si alloys [8-9] and the XRD results.

Fig. 5 shows the TEM bright-field micrographs of dendrites and interdendrites, and the corresponding selected area electron diffraction (SAED) patterns in the laser cladding coating. In Fig. 5(a), the bright regions in contrast correspond to the dendritic microstructure, and the dark regions, in contrast, correspond to the interdendritic microstructure. As shown in Figs. 5(b) and 5(c), the stronger reflections belong to the fundamental reflection, and the weaker reflections are the additional superlattice reflections. The existence of superlattice reflection confirms the existence of the ordering Fe_3Si phase. From the results stated above, it can be concluded that both the Si-rich dendritic microstructure and the Si-poor interdendritic microstructure correspond to the ordering $D0_3$ structured Fe_3Si.

Based on the characterization of the coating above, the solidification process can be analyzed as follows. During the laser cladding process, the liquid metal of mixed Fe and Si in the melt pool was rapidly cooled down, and there existed a high thermal gradient at the bottom of the melt pool. The Fe_3Si was formed as the nuclei of the dendritic microstructure, firstly, and then

grew fast towards the surface of the melt pool. The Si has a high solubility in Fe_3Si and during the growth of

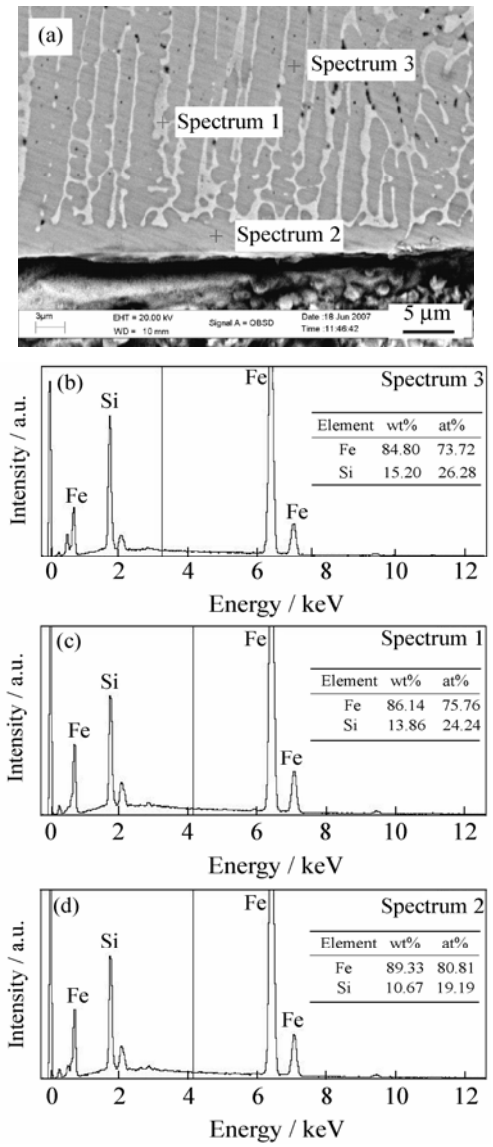

Fig. 4. SEM BSE micrograph of cladding coating (a) and EDS analysis of Fe and Si elements in the dendrite (b), interdendrite (c), and interface zone (d), respectively.

the Fe_3Si solid solution. During the growth of Fe_3Si, the Si content in the liquid metal around the dendrite decreased but to such an extent that the super cooled liquid metal was still in the same Fe_3Si phase region and then formed the Fe_3Si phase in the interdendritic region. Consequently, both the dendrites and the interdendrites are mainly composed of Fe_3Si phase. Generally speaking, as for the bcc structured Fe-Si phase with a high Si content, ordering needs elevated temperature or long-time annealing [10-11]. But the $D0_3$ structured Fe_3Si phase was formed because of the short time (tens of seconds) and high temperature (higher than 1500°C) annealing during the overlapping cladding process, which is similar to the flash annealing process [12]. In addition to the Fe_3Si phase, the γ-Fe(Si) phase, which is stable at high temperature, was retained at room temperature, without transformation to α-Fe(Si) because of the non-equilibrium effects of the rapid solidification in the laser cladding process. The Fe_5Si_3 phase was also the non-equilibrium phase formed because of the rapid solidification in the laser cladding process. In view of the small amount of γ-Fe(Si) phase and Fe_5Si_3 phase identified by XRD, it is not possible to observe them very distinctly in the microstructure by using OM, SEM, and TEM in the present work.

3.3. Hyperfine structure of the laser cladding coating

Transmission Mössbauer spectra of the Si steel substrate and the laser cladding coating at RT are shown in Figs. 6(a) and 6(b), respectively.

The Mössbauer spectra were fitted with the value of the hyperfine field combined with the XRD results of the coating. The fitting results of hyperfine parameters including isomer shifts (I.S.), quadrupole splittings (Q.S.), hyperfine fields (H_{hf}), and relative area (Area, %) of each subspectrum in the Fe-1Si substrate and the laser cladding specimens are listed in Tables 2 and 3, respectively.

The Fe-1Si substrate is mainly composed of α-Fe(Si) phase with two kinds of atom configuration of Fe–Fe and Fe–Fe(Si). In addition, the result obtained from the Mössbauer spectrum as shown in Fig. 6(a) also reveals there exists a small amount (about 3vol%) of FeSi phase in the substrate, which is not found in the XRD spectrum. This might be caused by the specimens for XRD and MS experiments taken from different locations.

Fe_3Si phase is ferromagnetic and its Mössbauer spectra can be resolved as two sets of six sharp lines, with the internal field H_{hf} of 31.06 and 22.12 T, respectively. Ordered Fe_3Si has a $D0_3$ structure, which can be described as four interpenetrating sublattices, with four different sites labeled as A, B, C, and D as shown in Fig. 7 [13]. Because the Fe atoms in the B sites, in Fe_3Si, are surrounded by eight Fe atoms in the 1st nearest-neighbor (NN) shell, and those in the A and C sites are surrounded by four Si atoms in the 1st NN shell; the higher hyperfine field value in the Mössbauer spectra is attributed to the Fe atoms in the B sites and the lower hyperfine field value is attributed to the Fe atoms in the A and C sites [14]. The results presented in Table 3 are in agreement with the previously reported results [10]. In the present work, a coating, consisting of approximately 93.9vol% Fe_3Si phase, was obtained under the optimized parameters.

Consequently, the high Si coating on the Fe-1Si substrate is the ordering $D0_3$ structured Fe_3Si-based coating.

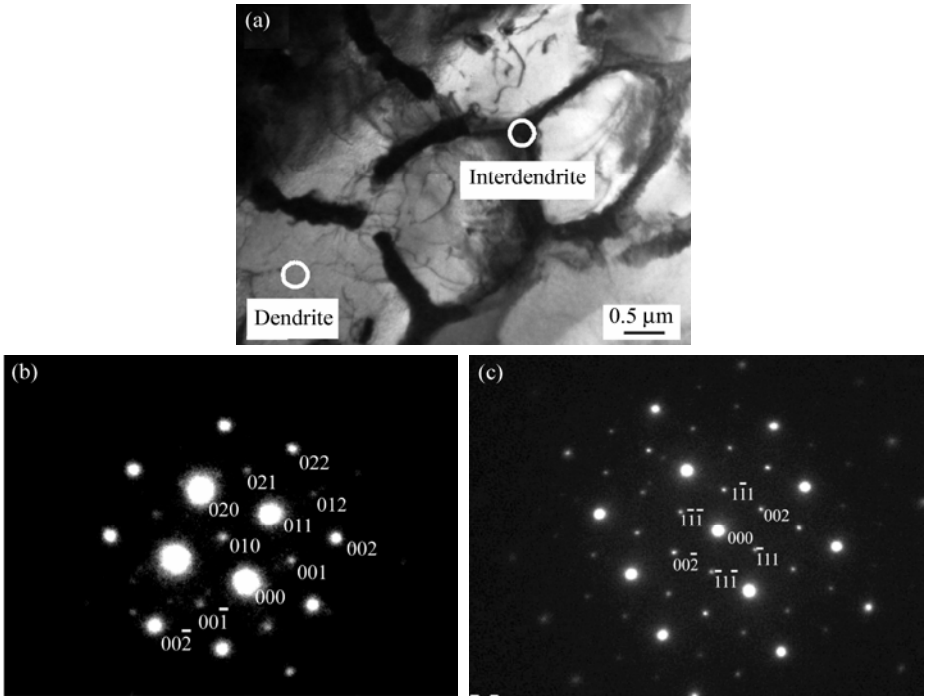

Fig. 5. TEM bright field micrographs of dendrite and interdendrite (a) in the laser cladding coating and corresponding SAED patterns of dendrite (b) and interdendrite (c).

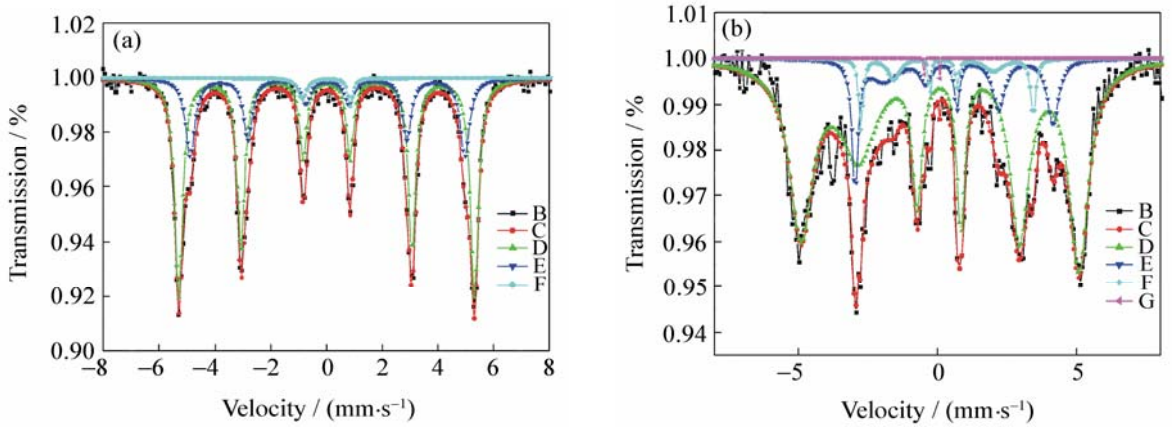

Fig. 6. Transmission Mössbauer spectra at RT of the Fe-1Si substrate (a) and the laser cladding Fe-Si coating (b).

Table 2. Fitting Mössbauer results of the Fe-1Si substrate

Subspectra	I.S. / (mm·s^{-1})	Q.S. / (mm·s^{-1})	H_{hf} / T	Area / %	Phase type	Atom configuration
1(D)	0.006	–0.002	33.01	68.3	α-Fe	Fe–Fe
2(E)	0.039	0.007	30.66	28.7	α-Fe	Fe–Fe(Si)
3(F)	–0.001	1.726	—	3.0	Fe-Si	FeSi

Table 3. Fitting Mössbauer results of the laser cladding Fe-Si coating

Subspectra	I.S. / (mm·s^{-1})	Q.S. / (mm·s^{-1})	H_{hf} / T	Area / %	Phase type	Atom configuration
1(D)	0.076	0.034	31.06	79.4	Fe-Si	Fe–Fe
2(E)	0.371	0.459	22.12	14.5	Fe-Si	Fe–Fe(Si)
3(F)	0.286	0.124	19.25	5.8	Fe-Si	Fe_5Si_3
4(G)	–0.204	0.563	—	0.3	γ-Fe	Fe–Fe(Si) –C

In addition, the hexagonal Fe_5Si_3 phase with $D8_8$ structure is also ferromagnetic and its Mössbauer spectra is a magnetic sextet with an internal field H_{hf} of 19.25 T, which is in agreement with the reported

value by Johnson, *et al*. [15] and Narasimhan, *et al*. [16].

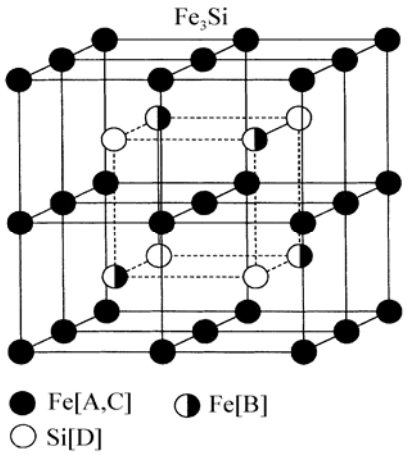

Fig. 7. Schematic diagram of the unit cell of the ordered Fe_3Si with $D0_3$ structure [13].

The subspectrum, as shown as the G line in Fig. 6(b), takes on a set of four pole peaks corresponding to the γ-Fe type phase in the cladding coating. And the Fe atom is surrounded by one C atom in the NN site, which leads to the lattice distortion and devastates the cubic symmetry of the lattice. Consequently, the value of Q.S. is not equal to zero in the case of γ-Fe type phase with the Fe–Fe(Si)–C atom configuration. And the γ-Fe phase is only, approximately, 0.3vol% in the coating, and it is hard to be observed by using OM, SEM, and TEM in the present work.

3.4. Magnetic property of the laser cladding coating

Fig. 8 shows the hysteresis loop of the laser cladding Fe-Si coating with the thickness of 0.18 mm measured at RT by using VSM. The distinct magnetic hysteresis loop at RT indicates that the cladding coating is ferromagnetic. This result agrees with the Mössbauer result that the cladding Fe-Si coating includes 99.7vol% ferromagnetic Fe_3Si and Fe_5Si_3 phases. The saturation magnetization (M_s), residual magnetization (M_r), and coercive force (H_c) of the cladding coating are 124.0 $A{\cdot}m^2{\cdot}kg^{-1}$, 1.1605 $A{\cdot}m^2{\cdot}kg^{-1}$, and 0.918 $kA{\cdot}m^{-1}$, respectively. The M_s, M_r, and H_c of the Fe-1Si substrate are 201.90 $A{\cdot}m^2{\cdot}kg^{-1}$, 0.0613 $A{\cdot}m^2{\cdot}kg^{-1}$, and 0.199 $kA{\cdot}m^{-1}$, respectively. Compared with the substrate, the cladding coating has a lower M_s value and a higher H_c value. The poor magnetic property of the coating might be because of the rapid solidification microstructure and the phase constitution in the coating. In this case, diffusion annealing after laser cladding is necessary for improving the magnetic property.

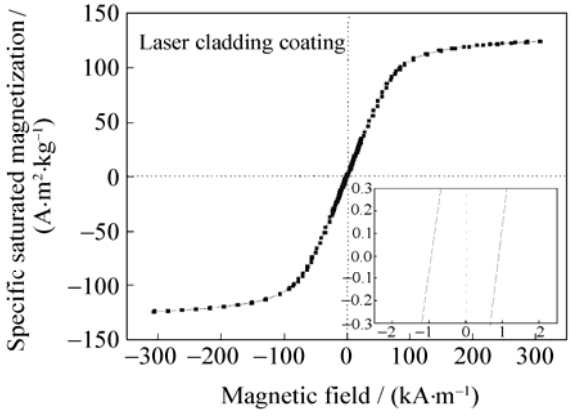

Fig. 8. RT hysteresis loop of the laser cladding Fe-Si coating with the thickness of 0.18 mm.

4. Conclusions

(1) A dense and crack-free cladding coating with an excellent metallurgical bonding with the Fe-1Si substrate was prepared by the optimized Nd:YAG laser cladding process. The microstructure of the coating is characterized by typical fine dendrites. And the Si content of dendrites and interdendrites are as high as 15.20wt% and 13.86wt%, respectively.

(2) The major phase of the laser cladding coating was confirmed to be the ordering $D0_3$ structured Fe_3Si phase, and Fe_3Si phase appears not only in the Si-rich dendritic zone but also in the Si-poor interdendritic zone, which are close in composition to Fe_3Si. In addition, there exists small amount of Fe_5Si_3 phase and γ-Fe phase.

(3) The M_s, M_r, and H_c values of the cladding coating are 124.0 $A{\cdot}m^2{\cdot}kg^{-1}$, 1.1605 $A{\cdot}m^2{\cdot}kg^{-1}$, and 0.918 $kA{\cdot}m^{-1}$, respectively. Compared with the Fe-1Si substrate, the magnetic property of the cladding coating is poor because of the rapid solidification microstructure and the phase constitution. And it is necessary to carry out diffusion annealing after the laser cladding process.

References

[1] T. Ros-Yañez, Y. Houbaert, O. Fischer, and J. Schneider, Production of high silicon steel for electrical applications by thermomechanical processing, *J. Mater. Process. Technol.*, 141(2003), No.1, p.132.

[2] Y. Ushigami, M. Mizokami, M. Fujikura, T. Kubota, H. Fujii, and K. Murakami, Recent development of low-loss grain-oriented silicon steel, *J. Magn. Magn. Mater.*, 254-255(2003), p.307.

[3] S. Sun, Y. Durandet, and M. Brandt, Parametric investigation of pulsed Nd:YAG laser cladding of satellite 6 on stainless steel, *Surf. Coat. Technol.,* 194(2005), p.225.

[4] D.Y. Dong, C.S. Liu, B. Zhang, and J. Miao, Pulsed Nd:YAG laser cladding of high Si content coating on low silicon steel, *J. Univ. Sci. Technol. Beijing*, 14(2007), No.4, p.321.

[5] D.Y. Dong, C.S. Liu, B. Zhang, and J. Miao, Effect of la-

ser cladding high Si coating on property of silicon steel, *Chin. J. Mater. Res.* (in Chinese), 21(2007), No.4, p.364.

[6] F. Alves, F. Simon, and O. Hubert, Analysis of both nanocrystallization and creep-induced anisotropy kinetics in Fe-Si-B-Cu-Nb alloys, *Mater. Sci. Eng. A*, 375-377(2004), p.1011.

[7] J.G. Jia, Q. Ma, J.J. Lv, Q. Zhou, G.S. Ji, and T.M. Guo, Preparation of ordered intermetallic compound of Fe_3Si with mechanical activation and sintering, *J. Lanzhou Univ. Technol.* (in Chinese), 33(2007), No.1, p.14.

[8] A. I1'inskii, S. Slyusarenko, O. Slukhovskii, I. Kaban, and W. Hoyer, Structural properties of liquid Fe-Si alloys, *J. Non Cryst. Solids*, 306(2002), p.90.

[9] F.J. Bolívar, L. Sánchez, S.A. Tsipas, M.P. Hierro, J.A. Trilleros, and F.J. Pérez, Silicon coating on ferritic steels by CVD-FBR technology, *Surf. Coat. Technol.*, 201(2006), p.3953.

[10] M.B. Stearns, Internal magnetic fields, isomer shifts, and relative abundances of the various Fe sites in FeSi alloys, *Phys. Rev.*, 129(1963), No.3, p.1136.

[11] Y.P. Yelsukov, V.A. Barinov, and G.N. Conygen, Influence of the order-disorder transition on the structural and magnetic properties of B.C.C. iron-silicon alloys, *Phys. Met. Metallogr.*, 62(1986), p.85.

[12] T. Kulik, T. Horubat, and H. Matyja, Flash annealing nanocrystallization of Fe-Si-B-based glasses, *Mater. Sci. Eng. A*, 157(1992), No.1, p.107.

[13] J. Kudrnovský, N.E. Christensen, and O.K. Andersen, Electric structure and magnetic moments of $Fe_{3+y}Si_{1-y}$ and $Fe_{3-x}V_xSi$ alloys with $D0_3$-derived structure, *Phys. Rev. B*, 43(1991), No.7, p.5924.

[14] G.A. Al-Nawashi, S.H. Mahmood, A.D. Lehlooh, and A.S. Saleh, Mössbauer spectroscopic study of order-disorder phenomena in $Fe_{3-x}Mn_xSi$, *Phys. B*, 321(2002), p.167.

[15] C.E. Johnson, J.B. Forsyth, G.H. Lander, and P.J. Brown, Magnetic moments and hyperfine interaction in carbon-stabilized Fe_5Si_3, *J. Appl. Phys.*, 39(1968), No.2, p.465.

[16] K.S.V.L. Narasimhan, W.M. Reiff, H. Steinfink, and R.L. Collins, Magnetism and bonding in a $D8_8$ structure; Mössbauer and magnetic investigation of the system Mn_5Si_3-Fe_5Si_3, *J. Phys. Chem. Solids*, 32(1970), p.1511.